Available online at www.sciencedirect.com
SCIENCE DIRECT®
International Journal of Mass Spectrometry 230 (2003) 185–192
International Journal of Mass Spectrometry
www.elsevier.com/locate/ijms

Calculation of the effect of collisional broadening on high-resolution translational energy loss spectra

A.G. Brenton*, P. Jonathan

Department of Chemistry, Mass Spectrometry Research Unit, University of Wales Swansea, Swansea SA2 8PP, UK

Received 29 August 2003; accepted 8 September 2003

To honour Professor John Herbert Beynon *FRS* on the occasion of his 80th birthday. Both the authors are indebted to John Beynon for providing intellectual guidance and practical experience in mass spectrometry. This paper, in particular, arose from ideas gained in the many sessions we had together discussing instrumentation and the experiments and science which would unfold with such new designs

Abstract

The collisional broadening of peaks in the spectra arising from translational energy spectroscopy (TES) studies is theoretically investigated. A numerical calculation, based on the TRIO matrix ion-beam transport computer programme, is used to simulate the collision event and its effects on the focussing properties of a number of 'double-focussing' instrument designs. The ion-optical models utilised include a commercial mass spectrometer and two novel high-resolution energy spectrometers (TESI and TESII), incorporating quadrupole and hexapole field lenses to focus the beam and reduce image aberrations. For a given design of spectrometer, peak broadening is evaluated in terms of the translational energy change suffered by the ion during collision and the angle through which it is scattered.

Keywords: Angle; Scattered; Collision

1. Introduction

A novel translational energy spectrometer was conceived out of one the many talks we had in John Beynon's Royal Society Research Unit. I (A.G.B.) gave a talk to the group one afternoon on a paper from Takieyo Matsuo's group, in Osaka, in which they described a compact time-of-flight mass spectrometer comprising four stigmatic-electrostatic sectors and described how we might adapt this for our energy loss work. At that time we were using a ZAB-2F (VG Micromass, Manchester, UK) on which we were having some difficulties getting high resolution. After discussions in the meeting and frantic discussions following that meeting, it became apparent that a double symmetrical electrostatic-analyser system would have excellent focussing properties for energy loss studies (refer to [1] for a comprehensive set of references on high-resolution translational energy loss spectrometry (TES)). A couple of years earlier, I had worked with Dr. Lester Taylor (Kratos Ltd., Manchester, UK) who had run most of the ion-optical simulations for Kratos. Lester and I worked on the optics for the double-electric sector design; the results of that work are described in [2]. The principal use of the two spectrometers, which we built in Swansea, TESI in 1987 [3] and TESII in 1994 [4], was to characterise the electronic and vibrational structure of ions and neutral species by precise measurement of the change in translational energy of keV ions colliding with a neutral target gas.

As early as 1982, Illies and Bowers [5] clearly demonstrated that a commercial high-resolution mass spectrometer could be used for TES studies, allowing an energy resolution of ca. ∼0.1 eV at 8000 eV collision energy. However, since our TESI spectrometer permitted even higher energy resolutions, it was anticipated that collisional broadening of energy loss peaks might prove to be a limitation, prompting the theoretical investigation reported here. In principle, the energy refocussing properties of the double-electric sector arrangement [1,2] are such that highly resolved images can be formed (∼10 ppm, measured at 5% peak height) when no gas is present in the collision cell. However, energy loss peaks arising from inelastic collisions with thermal gas targets are noticeably broader.

* Corresponding author. Tel.: +44-1792-295300; fax: +44-1792-295747.
E-mail address: g.brenton@swan.ac.uk (A.G. Brenton).

1387-3806/$ – see front matter © 2003 Elsevier B.V. All rights reserved.
doi:10.1016/j.ijms.2003.09.009

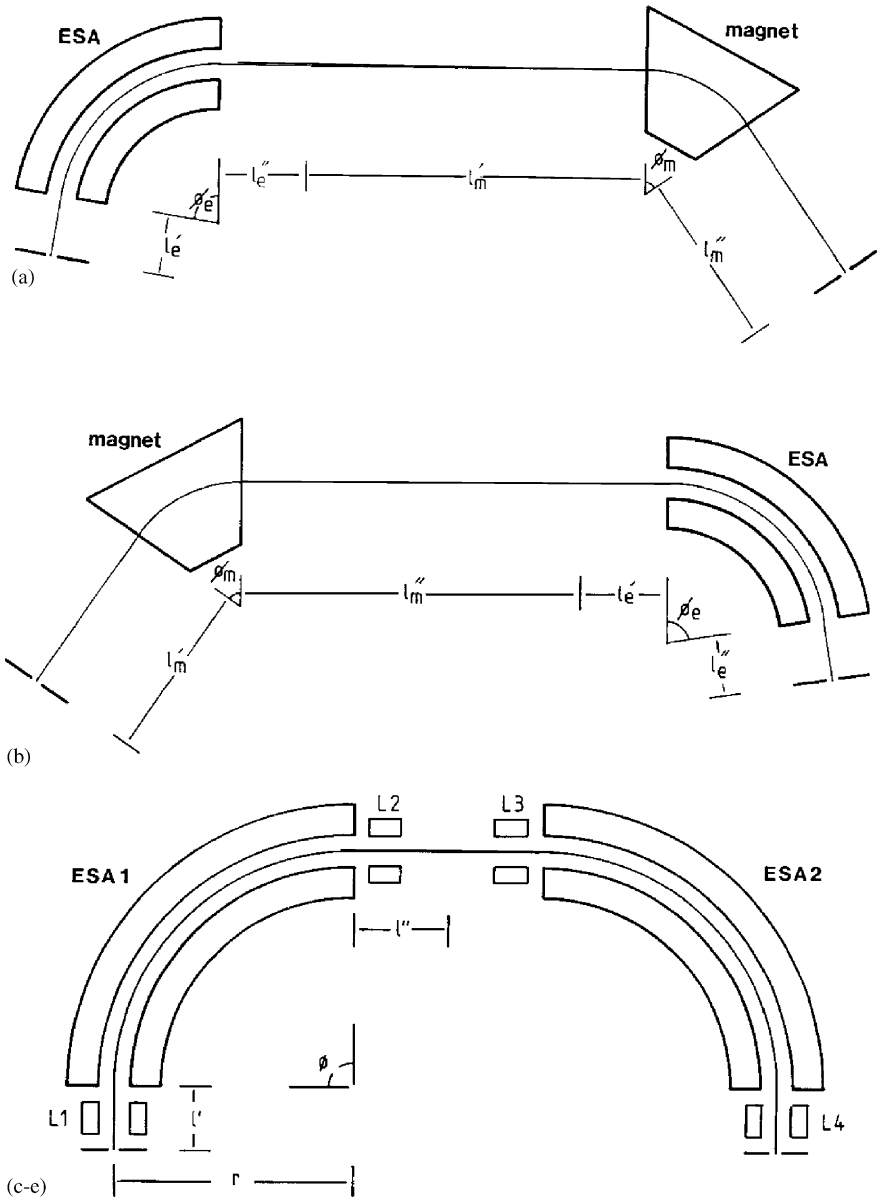

Fig. 1. Schematic diagrams of the translational energy spectrometer geometrics studied: (a) conventional Hintenberger and König geometry (design A); (b) reversed geometry Hintenberger and König (design B); (c) basic TESI geometry (no lenses h present) (design C); (d) TESI geometry with quadrupole lenses (L = Q) at L2 and L3 (design D); (e) TESI geometry with hexapole lenses (L = H) at L1 to L4 (design E).

Thus, the purpose of the present research is to predict the degree of broadening of a translational energy loss (or gain) peak, compared with the unscattered projectile beam, as a function of the main collision parameters (ε is the change in ion translational energy arising from a single collision; θ is the median plane scattering angle; $\varnothing$ is the scattering angle out of the median plane). In order to facilitate a comparison, two basic ion-optical designs, namely those of Hintenberger and König (referred to as the HK design) [6] and the TES double ESA [3] (referred to hereafter as the TESI design) are considered. As TESII is essentially a scaled-up version of TESI, we have not given detailed results of the expected collisional broaden for that instrument in this paper. For the HK design, conventional and reversed geometries are examined (refer to Fig. 1a and b). For TESI, a quantitative study of the use of various field lenses to reduce imaging aberrations due to intrinsic and collisionally induced ion-optical defects is undertaken. For the TESI design, it is assumed that a single focussing magnetic sector precedes the double-focussing arrangement of electric sectors, so that a mass selected ion beam enters the energy analysers. The collision process is modelled as a direct change of parameters, and its effect is calculated using the Third Order Ion Optics (TRIO) computer programme of Matsuo et al. [7], which we modified to include collisional broadening.

Theoretical modelling of ion-scattering processes in a mass spectrometer has been studied previously by Aleksandrov et al. [8–10] and Menat and coworkers [11,12].

The former were comprehensive studies of the scattering of an ion beam by residual gas in the analyser, including the effects of rough surfaces and collimating slits, using a Monte Carlo computer simulation. Both groups of authors report the tailing effect of ion-scattering on mass spectral peaks, along the whole flight path, and have not considered the effect of energy loss arising in collisions.

The present calculations predict that translational energy peaks can be significantly broadened due to the collision process, resulting in reduced energy resolution. Both the magnitude of the energy defect and the scattering angle for the collision greatly affect this broadening. It is noted that scattering in and out of the focal plane results in different amounts of image broadening. Consequently, methods of limiting peak broadening by the insertion of appropriate resolving and collimating slits, without excessive transmission losses, are suggested. Conclusions regarding the viability of the Hintenberger and König and TES designs as translational energy spectrometers are drawn.

2. Method

Trajectory calculations for a given ion-optical system can be undertaken by hand [13–15] or using a suitable computer programme or combination of programmes (e.g., TRIO [7], ION BEAM [16], GIOS [17], SIMION [18] and IonOpt [19]). Utilising the TRIO programme by a simple change of angle and energy parameters at the collision point, the aberration coefficients due to the collision are quickly generated. In current ion-optical nomenclature [20], the important ion trajectory parameters are

- x displacement of the ion trajectory from the central axis, in the focussing plane.
- y displacement of the ion trajectory from the central axis in the non-focussing plane.
- α half angle angular divergence of the ion beam in the focussing plane.
- β half angle angular divergence of the ion beam in the non-focussing plane.
- γ fractional mass spread in the ion beam.
- δ fractional energy spread in the ion beam.

Parameters x, α, y and β are functions of the ion-optical components of the system under consideration and can be numerically calculated at any point 'n' on the ion path. γ is a function of the sample used and δ of the ion source design, ripple on the acceleration voltage and operating conditions of the ion source. To study energy loss collisions, we assume that $\gamma = 0$ (in practice an ion of given mass-to-charge ratio is selected prior to energy analysis; scanning of the magnetic sector is not made); the relevant parameters can now be described in terms of the vector $I_n = (x_n, \alpha_n, y_n, \beta_n, \delta_n)$. In this context $n = 0$ refers to the object plane, $n = 1, 2$ to the collision point before and after collision, respectively, and $n = 3$ to the final image. TRIO facilitates the computation of numerical expansions for I_1 in terms of I_0 and I_3 in terms of I_2 of the form:

$$I_1 = (A, a, B, b, 1)I_0 \tag{1}$$

$$I_3 = (G, g, H, h, 1)I_2 \tag{2}$$

where (A, a, B, b, 1) represents the set of relationships:

$$\begin{aligned} x_1 = {} & A_X x_0 + A_A \alpha_0 + A_D \delta_0 + A_{XX} x_0^2 + A_{XA} x_0 \alpha_0 \\ & + A_{XD} x_0 \delta_0 + A_{AA} \alpha_0^2 + A_{AD} \alpha_0 \delta_0 + A_{DD} \delta_0^2 + A_{YY} y_0^2 \\ & + A_{YB} y_0 \beta_0 + A_{BB} \beta_0^2 + \text{third order terms} \end{aligned} \tag{3}$$

$$\begin{aligned} \alpha_2 = {} & a_X x_0 + a_A \alpha_0 + a_D \delta_0 + a_{XX} x_0^2 + a_{XA} x_0 \alpha_0 + a_{XD} x_0 \delta_0 \\ & + a_{AA} \alpha_0^2 + a_{AD} \alpha_0 \delta_0 + a_{DD} \delta_0^2 + a_{YY} y_0^2 + a_{YB} y_0 \beta_0 \\ & + a_{BB} \beta_0^2 + \text{third order terms} \end{aligned} \tag{4}$$

$$y_i = B_Y y_0 + B_B \beta_0 + \text{second order terms} \tag{5}$$

$$\beta_1 = b_Y y_0 + b_B \beta_0 + \text{second order terms} \tag{6}$$

$$\delta_1 = \delta_0$$

with the analogous expansions for I_3 in terms of I_2 denoted by (G, g, H, h, 1).

We now introduce a simple mathematical model for the collision process, so that expression of I_2 in terms of I_1 is possible. We assume that the collision produces a fractional increase in energy ε and angular deviations θ and ϕ, in and out of the median plane, respectively so that:

$$x_2 = x_1 \tag{7}$$

$$x_2 = \alpha_1 + \theta \tag{8}$$

$$y_2 = y_1 \tag{9}$$

$$\beta_2 = \beta_1 + \phi \tag{10}$$

$$\delta_2 = \delta_1 + \varepsilon \tag{11}$$

or

$$I_2 = (1, t, 1, p, e)I_1 \tag{12}$$

Eqs. (1), (2) and (12) can be combined to give

$$I_3 = (G, g, H, h, 1)(1, t, 1, p, e)(A, a, B, b, 1)I_0 \tag{13}$$

which can be rewritten as the sum of two expressions:

$$I_3 = (V, v, W, w, 1)I_0 + F \tag{14}$$

where

$$(V, v, W, w, 1) = (G, g, H, h, 1)(A, a, B, b, 1) \tag{15}$$

is independent of the collision parameters ε, θ and ϕ. That is, (V, v, W, w, 1) denotes the intrinsic aberrations of the ion-optical system, the most significant of which are the V_i terms ($i = X, A, D, XX, XA, XD, AA, AD, DD, YY, YB, BB$) expressing the final image width x_3 in the focussing plane,

Table 1
Expressions for the intrinsic aberration coefficients of a two stage ion-optical configuration

Values of ${}_iU_j$ (j)											
i	X	A	D	XX	XA	XD	AA	AD	DD	YY	YB	BB
X	A_X	a_X	–	–	–	–	–	–	–	–	–	–
A	A_A	a_A	–	–	–	–	–	–	–	–	–	–
D	A_D	a_D	1	–	–	–	–	–	–	–	–	–
XX	A_{XX}	a_{XX}	–	A_X^2	$A_x a_X$	–	a_X^2	–	–	–	–	–
XA	A_{XA}	a_{XA}	–	$2A_X A_A$	$A_x a_A + A_a a_X$	–	$2a_X a_A$	–	–	–	–	–
XD	A_{XD}	a_{XD}	–	$2A_X A_D$	$A_x a_D + A_d a_X$	A_X	$2a_X a_D$	a_X	–	–	–	–
AA	A_{AA}	a_{AA}	–	A_A^2	$A_a a_A$	–	a_A^2	–	–	–	–	–
AD	A_{AD}	a_{AD}	–	$2A_A A_D$	$A_a a_D + A_d a_A$	A_A	$2a_A a_D$	a_A	–	–	–	–
DD	A_{DD}	a_{DD}	–	A_D^2	$A_d a_D$	A_D	a_D^2	a_D	1	–	–	–
YY	A_{YY}	a_{YY}	–	–	–	–	–	–	–	B_Y^2	$B_y b_Y$	b_Y^2
YB	A_{YB}	a_{YB}	–	–	–	–	–	–	–	$2B_Y B_B$	$B_y b_B + B_b b_Y$	$2b_Y b_B$
BB	A_{BB}	a_{BB}	–	–	–	–	–	–	–	B_B^2	$B_B b_B$	b_B^2

The quantities ${}_iU_j$ are related to the actual aberration coefficients by Eq. (16).

in terms of the initial ion-beam parameters. The expressions for V_i to second order are given by:

$$V_i = {}_iU_j G_j \tag{16}$$

where ${}_iU_j$ are defined in Table 1.

F refers to Eq. (14) is a function of both I_0 and the collision parameters ε, θ and ϕ describing the aberrations of the ion-optical configuration entirely due to the collision event; when $\varepsilon = \theta = \phi = 0$, then $F = 0$. In a similar fashion to Eqs. (3) and (4), F can be expressed as the sum:

$$\begin{aligned} F &= F_T\theta + F_E\varepsilon + (F_{XT}x_0 + F_{AT}\alpha_0 + F_{DT}\delta_0)\theta \\ &\quad + (F_{XE}x_0 + F_{AE}\alpha_0 + F_{DE}\delta_0)\varepsilon + F_{TT}\theta^2 + F_{TE}\theta\varepsilon \\ &\quad + F_{EE}\varepsilon^2 + (F_{YP}y_0 + F_{BP}\beta_0)\phi + F_{PP}\phi^2 \end{aligned} \tag{17}$$

The form of the coefficients F of Eq. (17) are given in Table 2.

For the present calculations, the collision process is assumed to occur at the intermediate focal plane between the sectors of the double-focussing energy analysers, where the collision cell is located. Hence, the expression for (V, v, W, w, s) and F simplify because $A_A = G_A = 0$ and $V_D = 0$. The final image half width x_3 can be written:

$$x_3 = V_X x_0 + \Delta_V + F_E\varepsilon + \Delta_F \tag{18}$$

where Δ_V and Δ_F are the second order terms corresponding to intrinsic and collisional aberrations, respectively. The minimum fractional energy change, ε_0, detectable when the projectile ion beam (with translational energy to charge ratio U) suffers a change $U\varepsilon_0$ in translational energy to charge ratio, during collision, is

$$|\varepsilon_0| \le F_E^{-1}(V_X s + d + \Delta_0 + \Delta_c) \tag{19}$$

where s and d and the source and collector slit widths, respectively. Δ_0 is the sum of the absolute values of all the terms in Δ_V and is easily calculated once a set of maximum values of I_0, appropriate to the design, are chosen. In the present work, a reasonable set of values for beam width, angular divergence and energy spread are $x_{om} = 10^{-4}$ in., $\alpha_{om} = 10^{-2}$ rad, $y_{om} = 3 \times 10^{-2}$ in., $\beta_{om} = 10^{-3}$ rad and $\delta_{om} = 2 \times 10^{-3}$. The value of Δ_c depends on both the above maximum values and the collisional parameters ε, θ and ϕ so that the minimum separable energy change $U\varepsilon_0$ is a function of the collision process itself and can be expressed as:

$$\begin{aligned} \Delta_c &= C_E\varepsilon + C_T\theta + C_{EE}\varepsilon^2 + C_{ET}\varepsilon\theta \\ &\quad + C_{TT}\theta^2 + C_P\phi + C_{PP}\phi^2 \end{aligned} \tag{20}$$

General forms of the coefficients of C are given in Table 3.

Table 2
Expressions for the broadening aberration coefficients F of Eq. (17)

General expressions for F_i	
T	G_A
E	G_A
XT	G_D
AT	$G_{XX}A_X + 2G_{AA}a_X$
DT	$G_{XX}A_D + 2G_{AA}a_D + G_{AD}$
XE	$G_{XD}A_X + G_{AD}a_X$
AE	$G_{XD}A_A + G_{AD}a_A$
DE	$G_{XD}A_D + G_{AD}a_D + 2G_{DD}$
TT	G_{AA}
TE	G_{AD}
EE	G_{DD}
YP	$G_{YB}B_Y + 2G_{BB}b_Y$
BP	$G_{YB}B_B + 2G_{BB}b_B$
PP	G_{BB}

Table 3
Expressions for the coefficients C (Eq. (20)) in terms of the broadening aberration coefficients F

i	Expression
E	$\max\{\lvert F_{XE}\rvert\lvert x_0\rvert + \lvert F_{AE}\rvert\lvert a_0\rvert + \lvert F_{DE}\rvert\lvert\delta_0\rvert\}$
T	$\max\{\lvert F_{XT}\rvert\lvert x_0\rvert + \lvert F_{AT}\rvert\lvert a_0\rvert + \lvert F_{DT}\rvert\lvert\delta_0\rvert\}$
EE	$\max\{\lvert F_{EE}\rvert\}$
ET	$\max\{\lvert F_{ET}\rvert\}$
TT	$\max\{\lvert F_{TT}\rvert\}$
P	$\max\{\lvert F_{YP}\rvert\lvert y_0\rvert + \lvert F_{BP}\rvert\lvert\beta_0\rvert\}$
PP	$\max\{\lvert F_{PP}\rvert\}$

Table 4a
Geometric parameters for conventional and reversed geometry Hintenberger and König mass spectrometers designs

Ion-optical parameters	Conventional geometry (A)	Reversed geometry (B)
ρ_m	11.754	11.754
ϕ_m	55.000	55.000
ρ_e	15.000	15.000
ϕ_e	81°51′	81°51′
ℓ'_m	32.434	16.737
ℓ''_m	16.737	32.434
ℓ'_e	5.604	7.960
ℓ''_e	7.960	5.604

Refer to [6] for full details of the design; ρ: radius of a sector, ϕ: sector angle, ℓ': object distance, ℓ'': image distance, subscripts 'e' and 'm' refer to the electric and magnetic sectors, respectively. (All dimensions are in inches and all angles in degrees.)

3. Results and discussion

Using the simple collision model introduced above in conjunction with the TRIO computer programme, the intrinsic and collisional aberrations of five ion-optical systems were calculated. Together with the conventional and reversed geometry Hintenberger and König mass spectrometers (Fig. 1a and b and Table 4a), three versions of the TESI design were examined. (Fig. 1c–e and Table 4b) utilising various image correction devices, specifically included for second order aberration control, were studied. These five designs are referred hereon by A–E for ease of description:

A: conventional geometry Hintenberger and König (Fig. 1a and Table 4a).
B: reversed geometry Hintenberger and König (Fig. 1b and Table 4a).
C: basic TESI design (Fig. 1c and Table 4b).
D: TESI design incorporating two electrostatic quadrupole field lenses (Fig. 1d and Table 4b).
E: TESI design incorporating two electrostatic hexapole field lenses (Fig. 1e and Table 4b).

Mass spectrometer B is a commercial instrument (Vacuum Generators ZAB-2F [21]), previously used in our laboratory for such studies. Whilst design E is the instrument we constructed and used between 1987 and 1994 for high resolution energy loss studies. Currently we use its larger sister TESII.

In order to obtain high energy resolving power, inspection of Eq. (19) suggests a large value of F_E ($=G_D$), the energy dispersion of the post-collision analyser. However, in order to maintain symmetry of the double-focussing energy analysers which leads to very small image aberrations (i.e., $\Delta_0 \sim 0$), the first energy analyser would have to match the second. Additionally, the collisional aberration term Δ_c should be as small as possible. Although at first sight Eq. (19) would suggest the magnification V_X be small for a symmetrical arrangement it will be unity. To facilitate these calculations, the effects of magnetic sector fringing-fields were neglected in designs A and B in order to avoid having to make various assumptions concerning field terminations, e.g., Herzog shunts. Although all consequent calculations involving configurations A and B neglect magnet fringing-fields the results presented give good approximations to the actual design specifications. For cases C, D and E, the electrostatic fringing-fields were implicitly included, and we therefore expect high accuracy in these cases. On the further assumption that there is no mass spread in the ion beam ($\gamma = 0$), the relevant intrinsic aberration terms V_i for the five designs A–E are given in Table 5. Utilising these results, values of the total intrinsic aberration Δ_0 (expressed in units of microinch), to second and third order are given in Table 6. The higher order calculation is necessary especially for design E, for which third order aberrations are significant; because of its excellent second order focussing properties (refer to Table 5).

Similarly, the energy dispersion of the post-collision analyser, F_E, together with the collisional aberration terms C_i were calculated and are displayed in Tables 7a and 7b. Comparing F_E for the five designs A–E, we observe that designs B–E have similar values. F_E for design A is lower

Table 4b
Geometric parameters and electrostatic field lens strengths for the original TES design and those incorporating quadrupole (TES Q) and hexapole (TES H) lenses

Ion-optical parameter	TES	TES Q	TES H
ℓ'_e	4.585	4.468	4.585
ℓ''_e	6.000	6.000	6.000
ρ_e	15.000	15.000	15.000
ϕ_e	90	90	90
Sector half gap	0.5000	0.500	0.500
Lens strength	–	2.000	0.750
Lens displacement from ESA boundary	–	3.000	0.500
Lens strength	–	$Q1 = Q2 = 0.104$	$H1 = H4 = 0.0071$ $H2 = H3 = -0.0320$

ρ: radius of a sector, ϕ: sector angle, ℓ': object distance, ℓ'': image distance, subscripts 'e' and 'm' refer to the electric and magnetic sectors, respectively. (All dimensions are in inches and all angles in degrees. The lens strength for a $(2n + 2)$—pole is the value of the nth derivative of the corresponding electrostatic field evaluated on the optical axis $x = y = 0$.)

Table 5
Aberration coefficients for designs A–E (columns a–e) for second order correction

		(a)	(b)	(c)	(d)	(e)
x_0	x_2	0.655	1.526	1	1	1
	α_2	0.221	0.221	0.160	0.113	0.160
α_0	x_2	0	0	0	0	0
	α_2	1.526	0.655	1	1	1
γ	x_2	9.360	−14.286	–	–	–
	α_2	0.410	−1.799	–	–	–
δ	x_2	0	0	0	0	0
	α_2	−1.769	−1.160	−1.20	−0.518	−1.20
x_0^2	x_2	−0.250	−0.780	−0.360	−0.121	0.153
	α_2	0.005	−0.009	0.0041	0.0033	−0.0477
$x_0\alpha_0$	x_2	−2.998	−5.329	−4.51	−2.15	−1.91
	α_2	0.155	−0.102	0	0	0
$x_0\gamma$	x_2	−3.731	11.394	–	–	–
	α_2	−0.135	−0.005	–	–	–
$x_0\delta$	x_2	1.379	7.245	5.46	0.525	1.15
	x_2	−0.213	−0.033	−0.0589	−0.0123	1.35
α_0^2	x_2	1.706	−1.118	0	0	0
	α_2	4.066	0.982	2.25	1.07	0.955
$\alpha_0\gamma$	x_2	−28.816	20.153	–	–	–
	α_2	−1.023	−1.976	–	–	–
$\alpha_0\delta$	x_2	3.046	7.004	34.3	−0.569	−0.0542
	α_2	−2.185	−2.097	0.0299	−0.589	−1.15
γ^2	x_2	−6.753	−40.009	–	–	–
	α_2	−0.307	0.777	–	–	–
$\gamma\delta$	x_2	30.726	−60.854	–	–	–
	α_2	1.068	−0.030	–	–	–
δ^2	x_2	2.263	−12.346	−20.7	−0.147	0.0314
	α_2	1.259	0.961	0.212	−0.504	−10.80
y_0^2	x_2	−0.068	0.103	0	−0.0305	0
	α_2	−0.002	0.013	0	−0.0012	0.0581
$y_0\beta_0$	x_2	−10.085	4.330	0	−3.40	−0.0018
	α_2	−0.399	0.518	0	−0.132	3.97
β_0^2	x_2	−377.261	48.401	0	−80.3	−0.0619
	α_2	−11.672	6.638	1.2	−2.59	77.2

because of the poorer energy dispersion coefficient for the post-collision magnetic sector (Table 5). The numerical values of the coefficients C for the five designs demonstrate the superior performance of design E for collision processes with scattering in the y-plane; the coefficients C_P and C_{PP} are at least an order of magnitude lower for E than any of the other four cases. Indeed C_P and C_{PP} are so small for design E that they become negligible in comparison with C_T, C_{TT} and C_{ET}, which have comparable values for TESI designs C–E. The relatively poor performance of a conventional mass spectrometer for energy loss studies is highlighted in Tables 7a and 7b by the large values of C_P and C_{PP} for design A; these are indicative of the unique focussing properties of a magnetic sector.

Table 6
Numerical values of the maximum intrinsic aberration, Δ_0, calculated in 10^{-6} in. to second and third order correction

Order of approximation	Values of Δ_0				
	A	B	C	D	E
2	990	580	770	210	3.5
3	1000	610	860	710	210

Table 7a
Values of the broadening coefficients F

i	A	B	C	D	E
T	0.000	0.000	0.000	0.000	0.000
E	9.3360	14.300	14.700	14.600	14.700
XT	4.980	9.740	6.850	4.210	4.900
AT	36.600	40.200	54.000	51.000	48.700
DT	−15.700	−52.300	−52.800	−12.600	−29.400
XE	−3.740	−4.150	−2.830	−2.190	−3.000
AE	−28.900	−13.200	−15.800	−15.900	−14.000
DE	6.880	21.700	21.600	10.800	35.900
TT	−20.200	−34.000	−28.500	−26.000	−25.700
TE	31.900	22.200	16.700	16.200	14.800
EE	−6.750	−5.780	−5.410	−5.420	−8.490
YP	−5.360	0.000	0.000	−1.400	0.000
BP	−421.000	−28.700	29.400	−77.800	−0.885
PP	−117.000	−14.300	−14.700	−15.900	−0.458

The main results of the present calculations are shown in tabular form (Table 8) in terms of the minimum separable energy change UE_0 that can be detected by each of the designs A–E, for a collision process described by ε, θ and ϕ, at a projectile translational energy of 500 eV. Mass spectrometers such as A and B are not designed to operate at low values of U; their electrical stability, mass resolution, transmission, etc., are optimised normally around 8000 V. In contrast, the TESI spectrometer (C–E) has been designed to operate from 3000 eV down to 500 eV and from these calculations indicate the minimum energy changes (including collisional broadening) of 36, 32 and 14 meV can be separated, respectively. Hence, despite having similar ε_0 to the reversed geometry design B, the values of $U\varepsilon_0$ are significantly lower for C, D and E than B. For example, when $U = 500$ eV and $\varepsilon_0 = 200 \times 10^{-6}$, $U\varepsilon_0 = 0.1$ eV, whereas for $U = 5000$ eV and $U\varepsilon_0 = 1$ eV a 10-fold increase.

Realistic values of collision parameters, covering very soft to hard inelastic gas collisions, are assumed (ε = 10–10,000 meV; θ, ϕ = 10–1000 × 10^{-6} rad) in Table 8, permitting quantitative evaluation of the performance of each design. Table 8 gives the intrinsic $U\varepsilon_0$ for each design, indicating the superiority of spectrometer E which has an ultimate resolving power of ca. 14 meV. Table 8b and c, explore the dependence of $U\varepsilon_0$ an increasing collision

Table 7b
Values for the broadening coefficients C

i	A	B	C	D	E
E	0.300	0.180	0.200	0.180	0.210
T	0.400	0.510	0.650	0.540	0.550
EE	6.750	5.780	5.410	5.420	8.490
ET	31.900	22.200	16.700	16.200	14.800
TT	20.200	34.000	28.500	26.000	25.700
P	0.580	0.029	0.029	0.120	0.001
PP	117.000	14.300	14.700	15.900	0.460

Table 8
Minimum separable energy changes $U\varepsilon_0$ detectable using the ion-optical designs A–E for a collision process defined by ε, θ and ϕ

$U\varepsilon$ (meV)	θ (10^{-6} rad)	ϕ (10^{-6} rad)	$U\varepsilon_0$ (meV)				
			A	B	C	D	E
(a)							
0	0	0	64	30	36	31	14
(b)							
10	10	10	65	30	37	32	14
		100	68	31	37	32	14
		1000	102	32	38	36	14
		10000	1000	90	96	127	16
	100	10	67	32	38	33	16
		100	70	32	39	34	16
		1000	104	34	40	38	16
		10000	1002	92	98	129	18
	1000	10	87	49	59	51	34
		100	90	49	59	51	34
		100	124	51	61	55	34
		10000	1022	109	119	146	35
	10000	10	385	327	353	304	290
		100	388	327	353	304	290
		1000	422	328	355	309	290
		10000	1321	387	413	400	292
(c)							
100	10	10	68	32	38	33	16
		100	71	32	38	33	16
		1000	105	33	39	37	16
		10000	1003	92	98	128	17
	100	10	70	33	40	34	17
		100	73	33	40	35	17
		1000	107	35	41	39	17
		10000	1005	93	100	130	19
	1000	10	90	50	61	52	35
		100	93	51	61	52	35
		1000	127	52	62	57	35
		10000	1026	111	121	147	37
	10000	10	391	329	355	306	290
		100	394	329	356	307	290
		1000	429	331	357	311	290
		10000	1327	389	415	402	292
(d)							
1000	10	10	98	43	51	45	30
		100	101	44	51	45	30
		1000	135	45	52	49	30
		10000	1034	103	111	140	32
	100	10	101	45	53	46	31
		100	104	45	53	47	31
		1000	138	47	54	51	32
		10000	1036	105	113	142	34
	1000	10	104	64	75	65	50
		100	127	64	75	65	50
		1000	161	65	76	69	50
		10000	1059	124	135	160	52
	10000	10	453	355	379	328	313
		100	456	355	379	328	313
		1000	490	357	380	333	313
		10000	1388	415	439	423	315
(e)							
10000	10	10	533	234	247	230	274
		100	536	234	247	230	274
		1000	570	236	249	234	274
		10000	1468	294	307	325	276
	100	10	538	237	250	232	277
		100	541	237	250	233	277
		1000	575	239	252	237	277
		10000	1473	297	310	328	279
	1000	10	589	268	281	260	303
		100	592	269	281	260	303
		1000	626	270	283	264	303
		10000	1524	328	341	355	305
	10000	10	1194	686	677	613	648
		100	1197	686	677	613	648
		1000	1231	687	679	617	648
		10000	2129	746	737	708	650

The projectile translational energy is assumed to be $U = 500$ eV. The values of $U\varepsilon$ and $U\varepsilon_0$ are expressed in meV and the values of θ and ϕ in 10^{-6} rad.

translational energy change $U\varepsilon$ from 10 to 10,000 meV. Within Table 8b, the dependence of $U\varepsilon_0$ on scattering in (θ) and out of the plane of dispersion (ϕ) can be investigated. It is obvious from the tabulated results that the ϕ dependence of design A is considerable, compared with design E in particular. Also the relatively weak θ dependence of $U\varepsilon_0$ for design E supports its use as the basic model for mechanical construction. It should be noted, however, that at high collision energy changes in the region of 10 eV, the values of $U\varepsilon_0$ for each of the designs B–E are very similar, and not one of the geometries appears particularly superior.

In order to gain a better insight into the collisional broadening phenomena, a simple classical 'billiard ball' relationship of the form:

$$\Delta E = Um(P)m^{-1}(T)(\theta^2 + \phi^2) + U\varepsilon + \mathrm{o}(10^{-6})U \qquad (21)$$

was used to relate the collision parameters ε, θ and ϕ pertaining to a collision of a projectile of mass $m(P)$ with a target of mass $m(T)$ at an impact energy of U. ΔE is the energy defect for the collision.

With $U^{-1}\Delta E = \mathrm{o}(10^{-3})$, $m(T)m^{-1}(P) = \mathrm{o}(1)$, $\theta = \mathrm{o}(10^{-2}\,\mathrm{rad})$ and $\phi = \mathrm{o}(10^{-2}\,\mathrm{rad})$, Eq. (2) exhibits an error of order $(10^{-6})U$, as indicated; since $U\varepsilon$ is the translational energy gain of the projectile due to collision, then the first term on the right hand side must be the translational energy gain E_T of the target species:

$$E_T = Um(P)m^{-1}(T)(\theta^2 + \phi^2) + \mathrm{o}(10^{-6})U \qquad (22)$$

Thus, with Eq. (21), the relevant values of the parameters E_T, θ and ϕ pertaining to a collision between isobaric particles at $U = 500$ eV can be calculated and are given in Table 9. The values of θ and ϕ from this table clearly indi-

Table 9
Values of the scattering angles θ and ϕ appropriate to target translational energy gain E_T for inelastic collisions between impenetrable spheres of equal mass

E_T (meV)	θ (10^{-6} rad)	ϕ (10^{-6} rad)
0.1	0	447
	100	436
	316	316
0.5	0	1000
	100	995
	707	707
1	0	1414
	100	1411
	1000	1000
5	0	3162
	100	3161
	1000	3000
	2236	2236
10	0	4472
	100	4471
	1000	4359
	3162	3162
50	0	10000
	100	10000
	1000	9950
	7071	7071

The values of E_T are expressed in meV and θ, ϕ in 10^{-6} rad.

cate that even for small final target energies E_T, the scattering angles are appreciable. In particular for $E_T = 50$ meV, Table 8 suggests that none of designs A, B, C, D or E is capable of resolving $U\varepsilon = 10$ or even 100 meV for values of θ in the region of 0.01 radians. However, for smaller *x*-plane scattering ($\theta < 10^{-3}$ rad), then each of the translational spectrometers B–E can resolve $U\varepsilon = 100$ meV. This conclusion strongly suggests the use of beam collimators in the focussing plane to reduce the range of values of θ transmitted to the detector of the instrument. An experimental examination of the effect of such *x*-collimators is currently in progress.

4. Conclusion

Collisional broadening of translational energy spectra plays the dominant role in the determination of the ultimate energy resolving power of a translational spectrometer. For a given set of initial beam parameters $I_0 = (x_0, \alpha_0, y_0, \beta_0, \delta)$, a study of the effect of ion-beam scattering during inelastic collision processes has demonstrated that the ultimate separable energy change $U\varepsilon_0$ is primarily dependent on the scattering angles θ and ϕ pertaining to the collision, and not to the values of I_0, since it is the aberrations of the post-collision analyser that primarily limit resolution in product translational energy spectra. Therefore, in order to significantly reduce the effects of collisional broadening, a good double-focussing translational energy spectrometer, incorporating an angular-focussing post-collision energy analyser with negligible second order aberration terms, is desirable.

Acknowledgements

We thank the Science and Engineering Research Council, University of Wales Swansea and the Royal Society for support of this work. We also wish to express our gratitude to the late Professor T. Matsuo (Osaka) for providing us with the TRIO computer programme and to Professor J.H. Beynon and Dr. A.J.H. Boerboom for encouragement and helpful discussions and Dr. Chris Lock (Sciex, Toronto, Canada) who developed the TESII spectrometer.

References

[1] A.G. Brenton, Int. J. Mass Spectrom. 200 (2000) 403.
[2] J.H. Beynon, A.G. Brenton, L.C.E. Taylor, Int. J. Mass Spectrom. Ion Proc. 64 (1985) 237.
[3] (a) P. Jonathan, M. Hamdan, A.G. Brenton, G.D. Willett, Chem. Phys. 119 (1987) 159;
(b) M. Hamdan, A.G. Brenton, Chem. Phys: Phys. Ion Impact Phenomena 54 (1991) 165.
[4] C.M. Lock, A.G. Brenton, Rapid Commun. Mass Spectrom. 11 (1998) 1155.
[5] A.J. Illies, M.T. Bowers, Chem. Phys. 65 (1982) 281.
[6] H. Hintenberger, L.A. König, in: J.D. Waldron (Ed.), Advanced Mass Spectrometry, Pergamon, 1959.
[7] T. Matsuo, H. Matsuda, Y. Fujita, H. Wollnik, Mass Spectrosc. Jpn. 24 (1995) 19.
[8] M.L. Aleksandrov, L.N. Gall, N.S. Pliss, Zh. Tekh. Fiz. 44 (1974) 1302.
[9] M.L. Aleksandrov, N.S. Pliss, A.P. Shcherbakov, Zh. Tekh. Fiz. 47 (1977) 189.
[10] M.L. Aleksandrov, L.N. Gall, N.S. Pliss, A.P. Shcherbakov, Zh. Tekh. Fiz. 48 (1978) 1026.
[11] M. Menat, Can. J. Phys. 42 (1964) 164.
[12] M. Menat, G. Frieder, Can. J. Phys. 43 (1965) 152.
[13] E.G. Johnson, A.O. Nier, Phys. Rev. 91 (1953) 10.
[14] H.G. Voorhies, Rev. Sci. Instrum. 26 (1955) 716.
[15] H. Wollnik, Optics of Charged Particles, Academic Press, New York, 1986.
[16] D. Heck, E. Kasseckert, Kernforschungszentrum Karlsruhe Report K.F.K. 2379 (1976) 130.
[17] The General Ion Optical System (GIOS) ion beam transport computer programme of H. Wollnik has been cited, see for example, C. Brunnee, Int. J. Mass Spectrom. Ion Proc. 76 (1987) 125.
[18] D.A. Dahl, J.E. Delmore, Authors of the SIMION computer programme, Idaho National Engineering Laboratory, Idaho Falls, ID 83415, USA.
[19] J.H.J. Dawson, M. Guilhaus, Rapid Commun. Mass Spectrom. 3 (1989) 155.
[20] H. Nakabushi, T. Sakurai, H. Matsuda, Int. J. Mass Spectrom. Ion Phys. 52 (1983) 319.
[21] R.P. Morgan, J.H. Beynon, R.H. Bateman, B.N. Green, Int. J. Mass Spectrom. Ion Phys. 28 (1978) 171.